AIAA-91-3653

A Balloon-Borne Payload for Imaging Hard X Rays and Gamma Rays from Solar Flares

C.Crannell, B. Dennis, L. Orwig, E.Schmahl,
F. Lang, R. Starr and J. Norris
NASA GSFC, Greenbelt, MD

M. Greene
Auburn University, Auburn, AL
G. Hurford
Caltech, Pasadena, CA
W. Johnson and K. Wood
Naval Research Laboratory, Washington, D.C.

AIAA International Balloon Technology Conference
October 8-10, 1991 / Albuquerque, NM

AIAA-91-3653-CP

A BALLOON-BORNE PAYLOAD FOR IMAGING HARD X RAYS AND GAMMA RAYS FROM SOLAR FLARES

Carol Jo Crannell, Brian R. Dennis, Larry E. Orwig,
Edward J. Schmahl, Frederic L. Lang*, and Richard Starr*
Solar Physics Branch, Laboratory for Astronomy and Solar Physics
NASA Goddard Space Flight Center
Greenbelt, Maryland

Jay P. Norris
Laboratory for High Energy Astrophysics
NASA Goddard Space Flight Center
Greenbelt, Maryland

Michael E. Greene
Electrical Engineering Department
Auburn University
Auburn Alabama

Gordon J. Hurford
Solar Astronomy
Caltech
Pasadena, California

W. Neil Johnson and Kent S. Wood
Space Science Division
Naval Research Laboratory
Washington, DC

Abstract

Hard X rays and γ rays provide direct evidence of the roles of accelerated particles in solar flares. An approach that employs a spatial Fourier-transform technique for imaging the sources of these emissions is described, and the development of a balloon-borne imaging device based on this instrumental technique is presented. The detectors, together with the imaging optics, are sensitive to hard X-ray and γ-ray emission in the energy-range from 20 to 700 keV. This payload, scheduled for its first flight in June 1992, will provide 11-arc second angular resolution and millisecond time resolution with a whole-Sun field of view. For subsequent flights, the effective detector area can be increased by as much as a factor of four, and imaging optics with angular resolution as fine as 2 arc seconds can be added to the existing gondola and metering structures.

I. Introduction

Particle acceleration and the interactions of plasmas and magnetic fields are processes that occur throughout the Universe, signalling their presence by the high-energy electromagnetic radiations they emit. Solar flares, with their high fluxes at Earth and potential for multiwavelength observations, offer a unique opportunity to study these processes. Despite the significance of the hard X rays and γ rays produced in solar flares, virtually no direct imaging of these high-energy emissions has been available to answer even the most basic observational questions. High-resolution hard X-ray and γ-ray images will reveal the basic morphology of their sources, tell us how these sources evolve on physically relevant timescales, and enable us to determine how the propagation of energetic particles depends on their spectrum and the magnetic field structure of their sources.

The scientific potential of solar high-energy observations was demonstrated with results from instruments flown during the active phase of the previous solar cycle (1978 to 1984) on **NASA's Solar Maximum Mission (SMM)** and the **International Sun-Earth Explorer 3 (ISEE-3)**, the Japanese **Hinitori** satellite, the DoD **P78-1** spacecraft, and on high-altitude balloons. These observations showed that high-energy processes were at the core of the solar-flare phenomenon, and they provided a preview of what could be learned about flares with imaging in the hard X-ray and γ-ray domain. High-

*Also Department of Physics, The Catholic University of America, Washington, DC.

altitude, scientific ballooning offers an opportunity to develop and verify the required imaging technology while obtaining pioneering measurements of the sizes and locations of the high-energy sources in solar flares. The balloon payload described in this paper is the **High Energy Imaging Device (HEIDI)**. The characteristics and capabilities of **HEIDI** are summarized in Table 1.

TABLE 1.
Characteristics and Capabilities of **HEIDI**

Parameter	Value
Field of View	1° (whole Sun)
Number of Fourier Components	> 50, typical
Spatial Fourier Components	11 and 25 arc second
Energy Range	≤ 20 to 700 keV
Total Detector Area	128 cm^2
Total Effective Area	32 cm^2
Spectral Resolution	≤ 25% @ 100 keV
Image Contrast, strong sources	10:1
Sensitivity	~ 1/2 HXRBS
Operational Lifetime	1 day

The principal objective of the **HEIDI** Balloon effort is to enable imaging of solar flares in hard X rays and γ rays on angular size scales commensurate with fundamental processes responsible for these high-energy emissions. The payload is designed to be upgraded with more effective detector area and finer angular resolution as the required technology is developed. Observations with **HEIDI** also will serve to complement spatially resolved observations at microwave frequencies for characterizing physical parameters of the associated flare structures. Multiwavelength observations, spectrally and spatially resolved in both hard X rays and microwaves, will provide a capability never before available for investigating the basic physical characteristics of high-energy flare sources.

The instrumental approach on which the **HEIDI** payload is based is described in the following section, and descriptions of the payload subsystems are presented in Section III.

II. Approach

Hard X rays and γ rays cannot be reflected or focused by lenses or mirrors. Even grazing incidence reflection, used very effectively in soft X-ray astronomy, is impossible in the photon-energy domain above a few keV. What is required is a variation on the pinhole camera consisting of material opaque to these radiations, interrupted with transparent apertures. High-resolution imaging of solar flares in this domain requires individual apertures with sizes ranging from 50 microns to 3 mm in order to resolve sources with angular dimensions ranging from 2 arc seconds to 2 arc minutes. The corresponding material thicknesses range from 3 to 60 mm to provide maximum contrast while preserving a whole-Sun field of view with high-density materials such as tungsten.

Two methods for imaging hard X rays and γ rays are coded-aperture cameras and Fourier-transform collimator cameras. The advantages and disadvantages of each technique with respect to sensitivity and spatial resolution have been discussed in the Pinhole/Occulter Facility (**P/OF**) report (Tandberg-Hanssen *et al.*)[1]. We have chosen to pursue the Fourier-transform approach because of its ability to provide high spatial resolution images with X-ray and γ-ray detectors having moderate or no spatial resolution.

Descriptions of the Fourier-transform approach and some alternatives for its implementation are contained in Crannell *et al.*[2] and Prince *et al.*[3]. The technique utilizes an array of one-dimensional subcollimators, each measuring a different spatial Fourier component of the source. In the case of rotating grids (as for **HEIDI**), over a half rotation one subcollimator measures many Fourier components, all corresponding to the same spatial frequency but with a full range of orientations. Each subcollimator is comprised of a pair of grids separated by a large distance. The two grids that comprise each pair are identical to each other. Each grid is fabricated with a periodic array of apertures (slits) alternating with material opaque to hard X rays and γ rays (slats). The slit plus slat width of a grid is called the pitch. For the **HEIDI** balloon payload, the separation of the grids is 5.2 meters. As shown in Figure 1, the grids modulate the incoming X-ray flux. The amplitudes and phases of the modulated X-ray signal measure specific Fourier

components of the X-ray image. This information is the exact mathematical analog of that provided by a pair of radio antennas in a radio interferometer. Because of this direct, one-to-one correspondence, the analytic tools that have been developed and refined for radio interferometry will be used for analysis of the hard X-ray and γ-ray observations obtained with **HEIDI**.

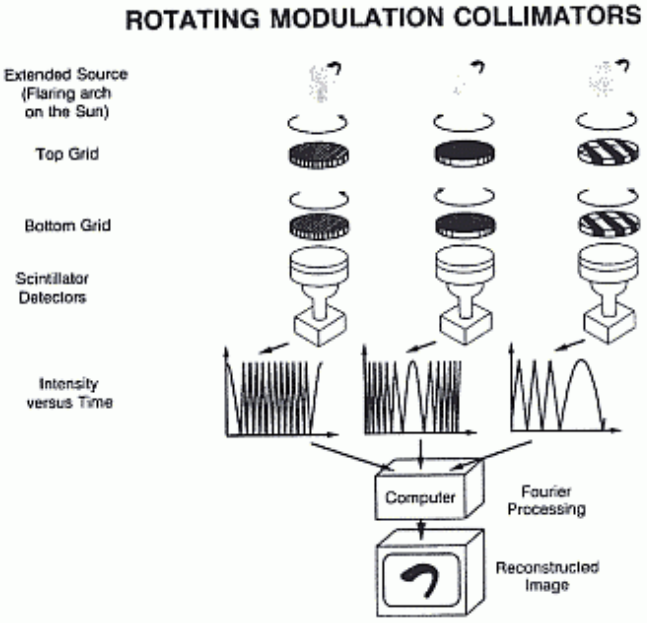

Figure 1. Schematic representation of the Fourier-transform technique used to obtain images of solar flares in hard X rays and γ rays with multiple rotating modulation subcollimators.

III. Payload Subsystems

A. Mechanical Structures and Alignment

The primary structural components of the **HEIDI** payload are the gondola, canister, and metering tubes, illustrated schematically in Figure 2. The gondola is a welded aluminum structure that weighs approximately 363 kg (800 lb). At its base it is 2.13 m (7 ft) wide on each side and at the top it is 1.50 m (4.9 ft) on each side. From the base to the top of the rotator housing the gondola is 6.52 m (21.4 ft) tall. It is fabricated in four sections that are bolted together. These are the lower deck or baseplate, two support towers and an upper deck which includes the azimuth rotator housing. The gondola is designed to allow rotation of the canister in elevation from 0 degrees to 90 degrees. Imaging of X-ray sources will not be possible over this entire range due to atmospheric absorption at low elevation and optical occultation by the balloon at high elevations. The full elevation range allows for alignment checks of the canister when horizontal and for vertical locking of the canister for launch and recovery to maximize survivability of critical instrument components.

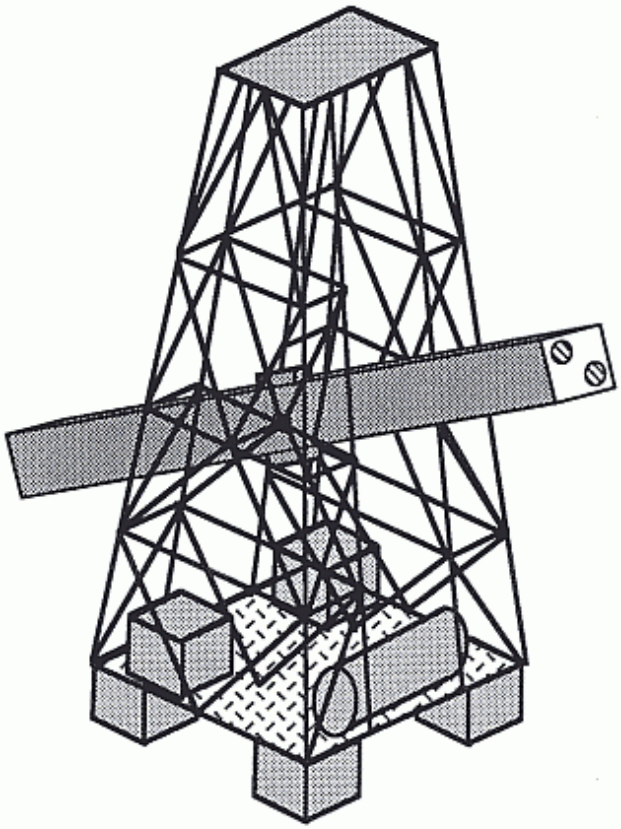

Figure 2. Schematic representation of the **HEIDI** payload shown without the rotator, crushpads, and flight-support equipment that will be provided by the National Scientific Balloon Facility.

The canister is a 5.2-m (17-ft) long frame reinforced rectangular (box-like) structure 0.61 m high x 0.51 m wide (24 in x 20 in). It is fabricated from titanium (Ti-6AL-4v) material which has a thermal coefficient of expansion close to that of the metering tubes. In addition to its external frame reinforcement, the canister has longitudinal reinforcement members in each of its corners. The structure is a riveted assembly of relatively thin face sheets (0.51 mm) compared to the thicker reinforcing members (2.54 mm).

The rectangular box-like structure is additionally reinforced by a series of four transverse aluminum bulkheads that are internal to the canister. The canister has one bulkhead at the forward end, one at the aft end, and two additional bulkheads near the center of the structure at the trunnion support points. These bulkheads maintain the rectangular shape of the

canister structure and support the metering tubes and their stepping drive motors.

The metering tubes are made of polyester fiberglass material. These tubes are nominally 5.2 m (17 ft) in length and are 152 mm (6 in) in diameter with a 3.2 mm (0.125 in) thick wall. They are used as torsionally stiff metering structures, employed to minimize the twist between the grid collimators located at each end.

B. Imaging Optics

The ultimate purpose of the canister and metering tubes is to hold the grid elements at each end of the metering tubes in the careful alignment required to make X-ray imaging possible. A 1-g structural analysis of the canister/metering tube assembly indicates that during flight the grid elements should deflect no more than:

- relative axial rotation: 0.9 arc minutes;
- relative rotation about a horizontal axis: 6 arc minutes; and
- relative transverse position translation: 0.44 mm.

The grids are fabricated from a tungsten alloy which has a density of 17.75 g/cm^3. Its composition by weight is 92.5% tungsten and 7.5% Ni/Fe. Each grid is cut from a blank which is 144 mm in diameter and 10 mm thick with a central active area 13.0 mm in diameter.

Fore and aft grids on each tube must be identical. Two different pitches, providing two imaging scales, are used. The finer grid has a pitch of 559 microns and a slit width of 330 microns. The coarser grid has a pitch of 1250 microns and a slit width of 625 microns. The slit/slat ratio of both pairs is 50/50, but other ratios can be selected based on a trade-off between throughput and modulation efficiency. The half-period of the fine and coarse grids are 11 arc seconds and 25 arc seconds, respectively, for a 5.2-m separation. A photograph of the first of the coarser grids to be fabricated is shown in Figure 3 as the slits are being cut with a traveling-wire Electric Discharge Machine (EDM).

C. Detectors and Analog Electronics

X-rays are detected at the aft end of each of the two grid collimator pairs with individual detector assemblies. Each assembly consists of a 90-mm diameter x 15-mm thick NaI(Tl) scintillator and a 90-mm diameter x 15-mm thick Schott SF1 lead glass optical window viewed with a 76.2-mm diameter Burle S83021EM1 photomultiplier tube with potted bleeder string. In addition, each assembly includes a mu-metal magnetic shield, Pb/Sn passive radiation shield, high-voltage power supply, and preamplifier. The energy resolution of each of the detectors is about 8% at 662 keV. A photograph of a detector assembly is shown in Figure 4.

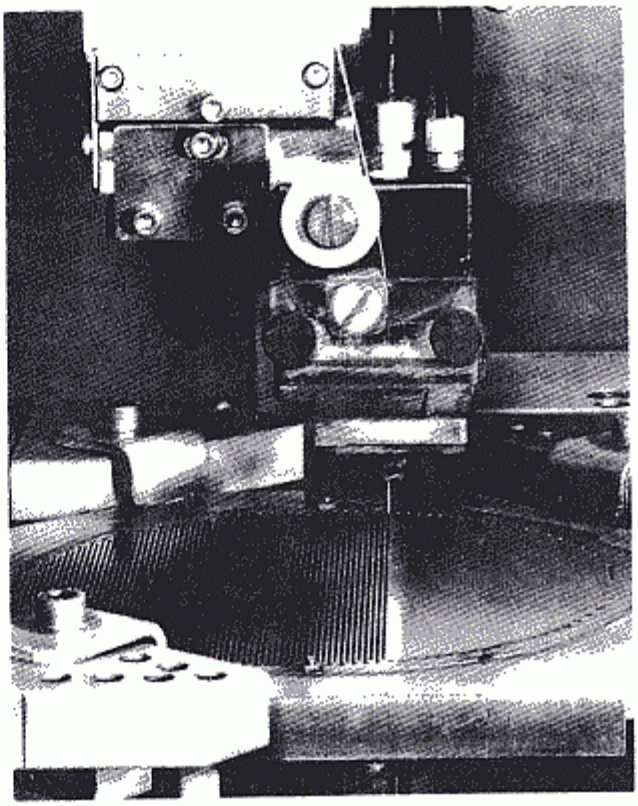

Figure 3. Photograph of 625-micron wide slits being cut in a 144-mm diameter by 10-mm thick tungsten-alloy blank with a traveling-wire Electric Discharge Machine.

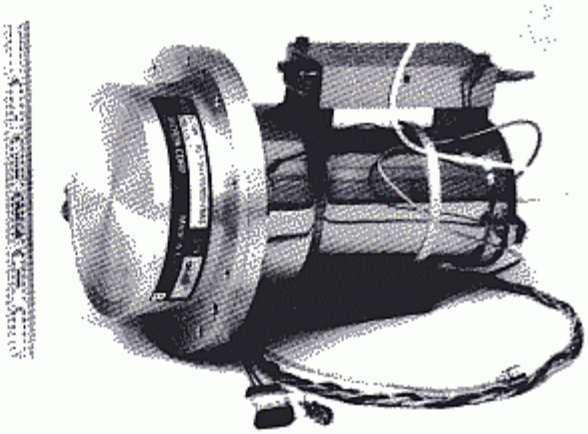

Figure 4. Photograph of a detector assembly.

The coarse gain of each detector assembly is controlled by adjusting the high voltage. High voltage adjustment is not possible during flight, but is done on the ground before flight. The high voltage and the gains of the preamplifier and shaping amplifier are selected so as to give an energy range of approximately 20 keV to 700 keV. The analog chain can support a maximum photon counting rate of 40,000 events/s.

D. Aspect and Pointing Control

The **HEIDI** aspect system determines the direction of the instrument optical axis relative to Sun center with an RMS (1 sigma) error of 0.2 arc seconds (which degrades the highest resolution X-ray amplitudes by at most 7 percent). A complete set of measurements can be made and recorded every 4 ms. A subset of these measurements are processed by an on board microprocessor to provide an error signal to the pointing system that is updated once every 40 ms. The field of view of this aspect system accommodates radial pointing displacements relative to Sun center of up to 15 arc minutes and permits acquisition from displacements up to 30 arc minutes.

The aspect system that meets these requirements consists of a filter and a 50-mm diameter, 5.2-m focal length lens mounted on the top grid plate. The 48-mm diameter solar image cast by the lens falls upon a hybrid chip containing four photo-diode detectors mounted on the lower grid tray, as seen in Figure 5. Each detector is a linear photo-diode pixel array of 2048, 15-micron pixels with a total active area of 100 mm x 0.015 mm providing a 2-dimensional positional readout of the image in video format.

Measurement of the location of the solar limb is simplified by the fact that a change in brightness of the solar image over the limb is large compared to the 10% RMS pixel-to-pixel sensitivity variation. This change in brightness will occur over 2 arc seconds or 4 pixels. Therefore, the nearest 0.5 arc second limb pixel can be identified by a binary comparison of pixel output with a fixed threshold. The RMS error in this process (without interpolation) is 0.17 arc seconds. Although this will be degraded when the limb is not orthogonal to the diode array, compensating analysis options include averaging of successive measurements (since pointing is likely to vary smoothly on sub-second time scales) and post-flight compensation for the relative pixel sensitivity.

Two digital feedback control loops govern the pointing of the telescope in both azimuth and elevation. Both control loops are housed in one

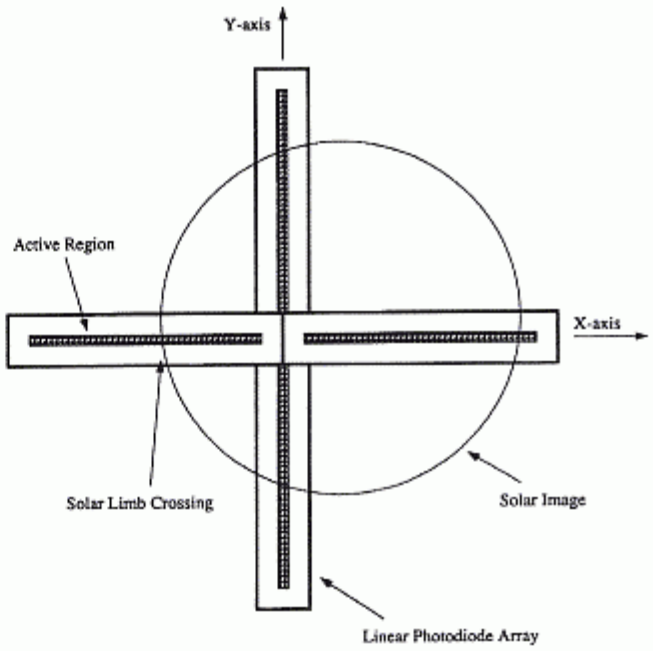

Figure 5. Layout of the optical aspect sensor showing the locations of the crossed, one-dimensional photo-diode detectors. The solid lines delineate the cases of the arrays. The narrower, cross-hatched regions indicate the active areas of the sensor. The circle represents a typical location of the solar image, offset from the optical axis, the location of which is the intersection of the vertical and horizontal arrays. The center of the image is determined from measurements of the limb crossings.

MC68HC11 microcomputer. The control loops were designed using pole-placement techniques with reduced order estimators. Each control system has three independent modes: acquisition, coarse pointing, and fine pointing. The aspect sensor serves as the sensor for fine pointing while a two-axis coarse Sun sensor with a ± 10 degree FOV serves as the sensor for coarse pointing. For acquisition, each axis has its own sensor.

In azimuth a direct drive servo torques against the balloon cable-ladder/parachute assembly to point the telescope and gondola at the Sun as well as damp cable ladder oscillations. A block diagram of the azimuth control system is shown in Figure 6. For acquisition, a tachometer is incorporated with the servo motor, and a constant rate loop is used until the coarse Sun sensor is activated. In azimuth, a total of 15 ft-lbs torque is available for pointing and slewing operations.

In elevation, a servo motor drives a ROTO-LOC^{TM} assembly which provides a zero backlash 30:1 reduction ratio for smooth operation in pointing the telescope relative to the gondola. For acquisitions

the elevation axis uses an encoder as a sensor and rotates the telescope to an angle which is commanded by uplink. The elevation control loop is essentially the same as the azimuth loop of Figure 6 without the cable ladder dynamics. A total of 30 ft-lbs torque is available in the elevation axis.

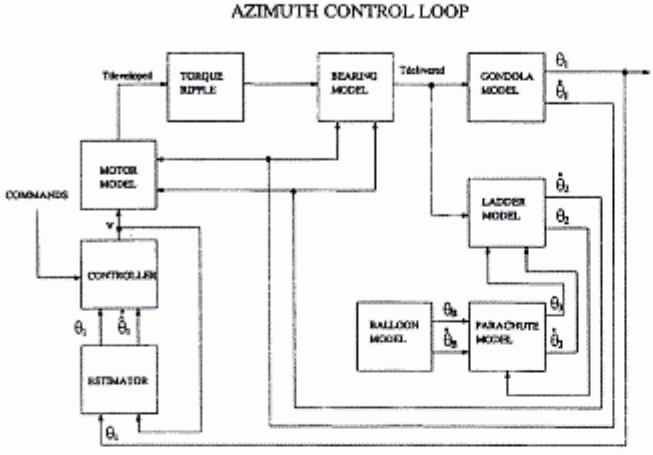

Figure 6. Block diagram of the **HEIDI** azimuth-pointing control loop. Both the controller and estimator are realized in software using a MC68HC11 μ computer.

E. Off-Pointing Aspect System

A key objective of the first flight is to verify the imaging properties of **HEIDI** for a point source. This will be accomplished by observations of the Crab nebula. Two sets of images will be made, one using windowed data when the 33 ms Crab pulsar is on, and one when the pulsar is off. The difference in these images will represent the response to the pulsar and will be used to confirm the spatial point-response function of the system. In addition, the images themselves will provide the highest resolution maps yet obtained of the Crab nebula at hard X-ray energies.

An Off-Pointing Aspect System (**OPAS**) provides the high-resolution aspect information necessary for the Crab observations. The first component of **OPAS** measures the radial offset of **HEIDI**'s optical axis with respect to Sun center and provides the necessary real-time feedback to the pointing system. The requirements of day-time observations, arc second precision and modest cost ruled out startrackers, magnetometers and gyros for this application. The chosen system makes use of a second lens on the front grid plate. This lens is preceeded by a pair of prisms, whose orientation can be adjusted prior to launch. Since each prism deflects a beam up by 10 degrees, their combined setting can deflect a beam to any angle within a 20 degree radius, as in a laser beamsteering system. In this case, the prisms and the lens focus an offaxis solar image onto the solar aspect sensor. The solar aspect system then tracks the Sun while the X-ray optics view the Crab. This is possible for a two hour period for each day within a 40 day launch window. Note that this system provides RELATIVE aspect for Crab viewing; *ABSOLUTE* aspect is not required since the location of the pulsar is known *a priori*.

Still to be dealt with is the measurement of roll about the Earth-Sun line, which will be affected by pendulation of the suspended payload. The anticipated amplitude of pendulation is sufficiently small (~0.1 degree RMS) that neither tracking the Crab nor the solar aspect solution will be affected adversely. Pendulation at this level, however, can seriously degrade the aspect solution for Crab observations. To remove its effects, it is necessary to monitor the roll angle of the canister about the Earth-Sun line. This is accomplished by the second component of the **OPAS** system, namely an off-pointing video camera which views a bright star (Sirius) whose image is recorded on a SVHS tape recorder. Post analysis of the motion of the stellar image will provide a continuous record of relative roll during the 2 hours of Crab viewing. Backup transmission of the images for ground recording will use an independent video telemetry link.

F. Flight Electronics

A block diagram of the **HEIDI** flight electronics is shown in Figure 7. The overall **HEIDI** flight electronics system can be divided into the following ten functional subsystems:

- Data handling, data merging, and data storage system;
- Analog and digital housekeeping data collection system;
- Telemetry formatter and NSBF data interface system;
- Payload azimuth/elevation pointing control system;
- Solar aspect system;
- Power conversion and distribution system;
- Commands interface and distribution system;
- Offpoint Aspect System (**OPAS**);
- Thermal control system for telescope and pressurized flight electronics; and
- Dual RMC tube motor driver and position encoder system.

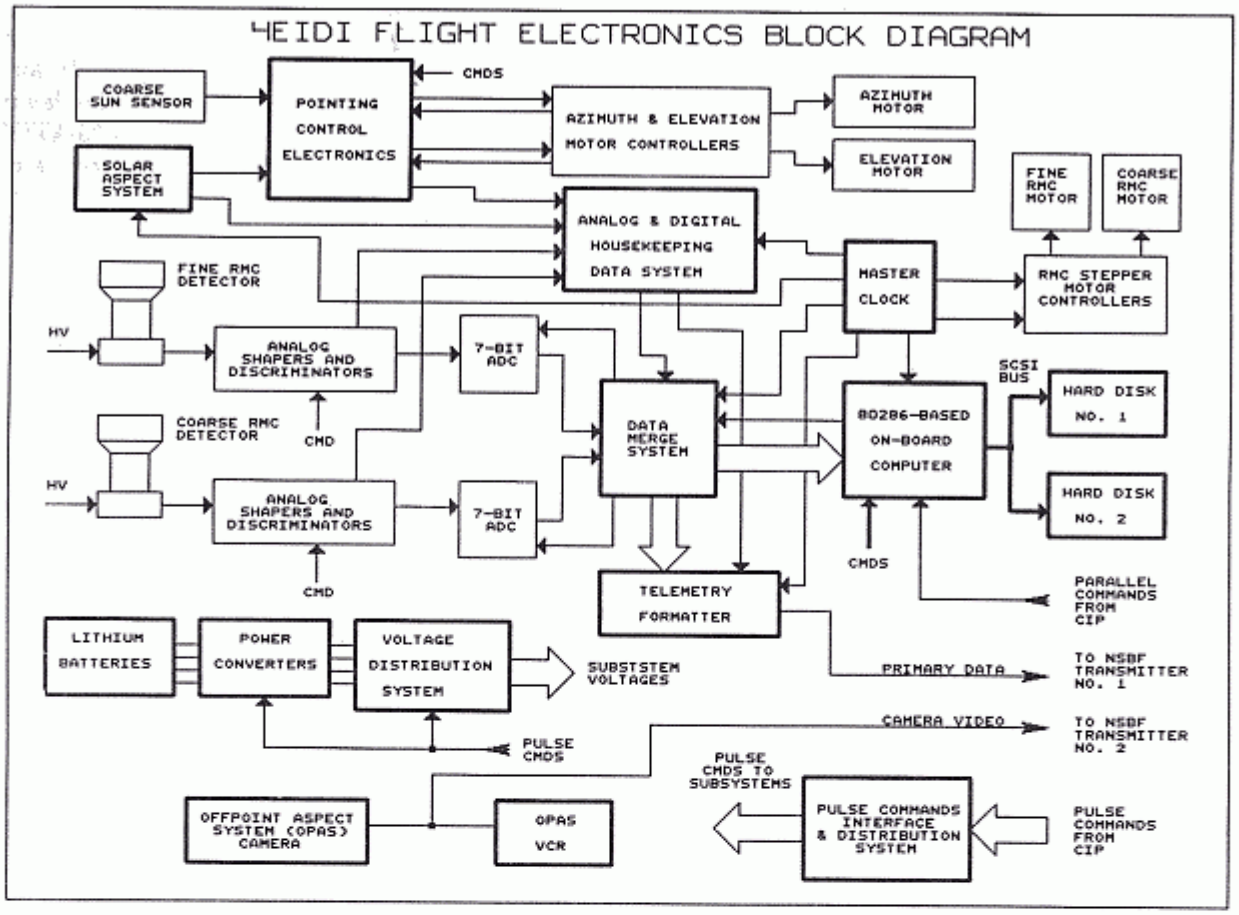

Figure 7. Block diagram of the **HEIDI** flight electronics, showing only the science payload electronics systems.

The principal function of the data handling system is to accept digital data from the detectors and fine aspect system, to merge this data with engineering housekeeping data, and to buffer and format these data for on-board recording on two high-capacity SCSI hard disk drives. The heart of this subsystem is an 80286-based on-board computer that provides two basic functions: it 1) formats, buffers, and transfers the merged science and housekeeping data to the dual SCSI on-board hard disk drives, and 2) interfaces the NSBF parallel command system to the payload and distributes these commands to the various electronic subsystems. A fixed sample of the total data is also formatted by a microprocessor-based telemetry formatter and NSBF data interface system and, telemetered to ground at a 200 kilobits/s rate in real time. This provides the capability of monitoring the health and safety of the payload as well as providing the ability to perform some near real-time data analysis during the mission.

The digital science data system utilizes a photon-tagging scheme that tags each detected photon with its absolute arrival time to 0.1 ms, its energy with 7-bit resolution, and the detector identification. In addition, solar aspect information produced by the fine solar aspect system is recorded with 20 ms time resolution. This photon and aspect information is utilized in the post-flight data analysis to calculate the Fourier amplitude and phase components needed to produce images. The data handling system is capable of processing 40,000 photon events per second per detector, which makes it well suited to handle intense flares. The total storage capacity of the on-board hard disks is 600 Mbytes.

The science payload power system utilizes lithium batteries as the primary power source. Subsystem power is obtained by using a combination of standard DC-DC converters and series pass regulators and is switched to the various subsystems using ground-commanded latching relays. The 1000 watt capacity

of the power system is sufficient for a two day mission. All critical subsystem and battery voltages and temperatures are monitored on board with a dual microprocessor-controlled analog and digital engineering data housekeeping system that is capable of monitoring 128 separate analog parameters. Data collected by this system is merged with primary science data to produce the complete data stream.

The RMC tube drive system contains the electronics to rotate synchronously the two collimator tubes at a constant rate of 1 rev/5 seconds by using a stepper-motor driven reduction gear and timing belt driver system. A slotted wheel/optical-sensor position-encoder system monitors the angular position and rotation speed of each of the four collimator grids. These data are collected with the housekeeping data system. A separate sensor system monitors the relative twist of the fore and aft mounting plates about the telescope bore-sight axis to an accuracy of 30 arc seconds.

The **HEIDI** pointing control subsystem consists of a microprocessor-based digital closed-loop servo system which provides two-axis pointing in azimuth and elevation. The pointing system includes the digital electronics combined with azimuth and elevation motor controllers and motors. Pointing error signals are provided by a coarse Sun sensor during initial solar acquisition, by the fine solar aspect system during the normal solar observing mode, and by **OPAS** during the Crab Nebula observing period. The operational mode of the pointing system (whether solar observing or solar offpoint mode) is selected by ground command. Once the mode is chosen, the pointing control system operates stand-alone without ground intervention. The capability exists in the flight electronics to modify the on-board pointing control software in real time by ground command if required.

A final electronics subsystem is the thermal control system that will maintain the overall telescope temperature above an optimum level and also maintain the fore and aft grids to within two degrees of each other at all times during the mission. The system operates in a closed-loop mode using battery-powered strip heaters controlled by thermostats and a thermister-driven differential temperature control circuit.

G. Data Acquisition and Ground Support Equipment (GSE)

The **HEIDI** GSE is based on a MicroVAX 3300 minicomputer with the capability of accepting data from the payload in several different ways at different stages of the program. The basic block diagram of the GSE is shown in Figure 8, and its interconnections to the payload command and data handling system are shown in Figure 9. During flight the bi-phase bit stream from the flight telemetry formatter is directed to the on-board transmitter and transmitted to the NSBF receiver at the ground station at 200 kbits/s. This serial bit stream is converted to a 16-bit parallel mode with a standard bit synchronizer and frame synchronizer and fed into the MicroVAX through a DRQ3B interface board. For test purposes on the ground, the transmitter and receiver can be bypassed with a coaxial cable. The data written to the flight hard disks can be read in to the MicroVAX through the SCSI link indicated in the block diagram.

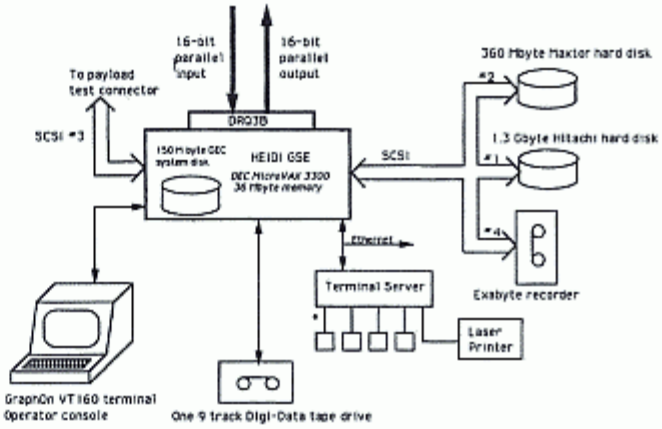

HEIDI GSE Computer

Figure 8. Block diagram of the **HEIDI** GSE Computer.

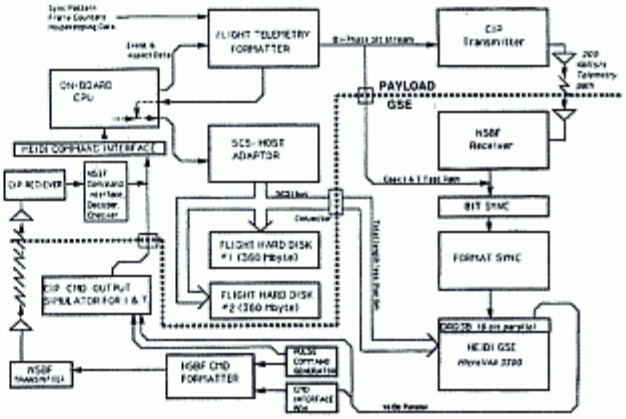

HEIDI Payload - GSE Interface

Figure 9. Block diagram of the computer/payload interface.

Data received with the MicroVAX is immediately written to the 1.3-Gbyte hard disk in the same format

as that used for the data written to the on-board hard disks. This requires some reformatting of the telemetry data. All data are eventually archived using an Exabyte tape recorder. The maximum amount of data per day of full time operations will be 2.1 Gbytes. Thus, we expect to be able to store all the flight data on the hard disk assuming an 8-hour flight.

During data collection, only a small amount of data can be displayed and analyzed. Page displays of selected payload characteristics are available to verify the health and safety of the instrument and the correct operation of the pointing control system and the aspect system. Some simple data accumulation and plots of time variations and X-ray spectra also will be possible in real time. More complex analysis including spectral deconvolution, phase plots, and statistical studies can be carried out by reading the data back from the 1.3 Gbyte hard disk in near real time. The analysis required to obtain images at different times during the flight and at different energies also can be carried out on the GSE MicroVAX but at a much slower rate. The final detailed analysis of all flight data will be carried out on larger VAX computers at GSFC and Caltech.

Pulse and 16-bit serial commands can be sent to the payload from a command generator box via the NSBF command formatter, transmitter, and on-board receiver and decoder. Serial commands can be generated in the MicroVAX and transmitted in the same way. For ground-based testing, the NSBF equipment can be bypassed using a command output simulator connected directly to the on-board command interface unit.

H. Data Reduction and Analysis

The primary data from **HEIDI** consists of the set of time-tagged photon events that identify the subcollimator and energy of each photon, and the time of its detection. The aspect solution can be interpolated to yield the pointing direction and orientation of the subcollimator at the time of detection of each photon. The task of converting this data stream into X-ray images can be conveniently divided into two stages. For the sake of discussion, we assume that an energy and time interval has been identified for the desired X-ray image. For convenience, an arbitrary point within the area to be mapped is designated as the "phase center".

The objective of the first stage is to determine a set of calibrated amplitudes and phases, each of which measures a Fourier component corresponding to the average of a small range of orientations of one subcollimator. For each component, this is accomplished by first identifying the subset of photon events that satisfy the combined energy, time, subcollimator, and subcollimator orientation criteria. The aspect solution is then applied to identify the locus of positions on the sky which correspond to the most likely origin of each photon. This locus is characterized by a projected distance from the phase center orthogonal to the grid orientation and modulo the angular pitch of the subcollimator. For each photon, the locus can be expressed as a phase (modulo 360 degrees). For example a photon whose most likely location of origin included the phase center would be assigned a phase of 0 degrees. If its most likely origin had a projected displacement of one half of the angular pitch (or 3/2 pitch, ...), its assigned phase would be 180 degrees. Each photon is also assigned a unit amplitude that can be weighted to take into account dead-time and other such instrumental corrections. In this manner, each photon is represented by a phasor. The set of phasors is then summed vectorially to yield the resultant amplitude and phase. It can be shown[3] (Prince *et al.*) that this represents a Fourier component of the source distribution.

With the set of measured amplitudes and phases determined, the second stage of the imaging task becomes identical to that in radio interferometry in which the maps are generated from measurements of amplitudes and phases determined from the correlation of signals from separate antennas. To this end, standard techniques[4] (Thompson, Moran, and Swensen) of Fourier inversion including CLEAN and Maximum Entropy Method can be employed using existing software packages such as AIPS.

I. OPTICAL IMAGING

Although testing and calibration at the subsystem level will verify that critical alignment requirements have been met, a prelaunch end-to-end test of the imaging system is highly desirable. This will be accomplished by optical imaging of a bright star (Sirius) from the ground. For this purpose, each scintillation detector will be replaced by a photomultiplier tube, whose scaled pulse train output will be fed into the **HEIDI** data system in the same manner as X-ray counts. The output of the phototube will represent the sum of unmodulated signals from dark current and diffuse sky emission and the signal from the star which will be modulated by the rotating collimators. The fixed attitude of **HEIDI** will be compensated by synthetic aspect data which will account for the known sidereal drift of the star.

Although the primary goal will be the recovery of the point source image of the star, analysis outputs also will include a comparison of the modulation amplitudes for the fundamental and third harmonics with the average signal enhancement as the star passes across the field of view; and the behavior of phase and amplitude response as a function of grid position angle and location of star. Additional diagnostic data can be obtained by selective masking of upper and lower grid areas.

The feasibility of such an optical calibration depends, of course, on alleviating the effects of diffraction by the grids. Starting from Lindsey's analysis of diffraction in multigrid systems,[5] it can be shown that the effect of diffraction is to multiply the modulation amplitude in a bigrid system by a "diffraction factor", D, which is given by:

$$D = cos(\frac{\pi L h^2 \lambda}{p^2})$$

where L is the separation of the grid planes (=5200 mm), p is grid pitch (=1.25 or 0.559 mm), h is the harmonic under consideration (=1 or 3) and λ is the wavelength of the incident plane wave. Figure 10 shows how the diffraction factor varies with wavelength for cases of interest. Although a conventional diffraction limit might be considered to be the shortest wavelength at which the amplitude is reduced by 50% (*e.g.*, 200 Angstroms for the fundamental harmonic and finest grid), Figure 10 shows that at selected longer wavelengths, the effects of diffraction again become unimportant. This occurs when the separation of the diffraction maxima formed by the upper grid becomes commensurate with the period of the lower grid. Thus full modulation can be obtained at long wavelengths provided one uses a sufficiently narrow bandwidth centered about an appropriate wavelength. In this case a 50 Angstrom filter centered about 6010 Angstroms is a viable choice.

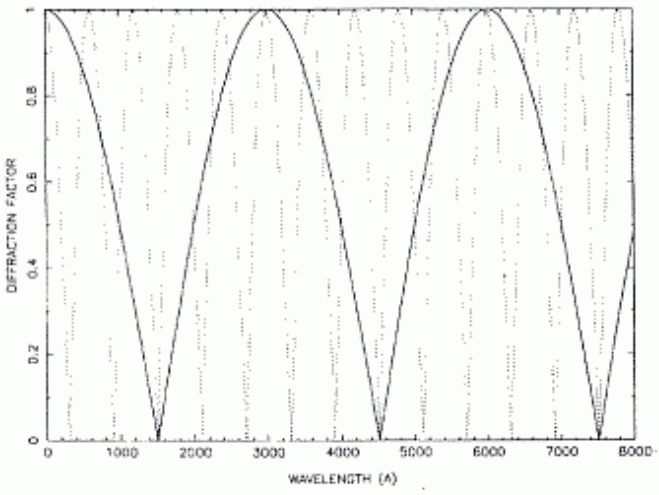

Figure 10. Factor by which modulation amplitude is reduced by diffraction for **HEIDI**'s coarse and fine grids (solid and dotted lines respectively) at optical wavelengths. In alternate maxima, the phase of the modulation is reversed.

IV. Summary and Conclusions

High-altitude, scientific ballooning, with its heavy-lift capability and the cost-effective approaches for the fabrication of payloads that it enables, offers unique opportunities for the development of new technologies and the pursuit of new and exciting science. Hard X-ray and γ-ray imaging technology is now being developed with the **HEIDI** balloon payload. X-ray and γ-ray spectroscopic capabilities are being developed with the High Resolution Gamma Ray Spectrometer (**HiREGS**) balloon payload that will be flown on long-duration balloon flights from Antarctica as part of **NASA**'s Max '91 Program. Together, these technologies provide the basis for the High Energy Solar Physics (**HESP**) Mission that has been studied for possible space-flight opportunities during the solar maximum that will begin in approximately the year 2000.

V. Acknowledgments

The instrumental concepts described here have been stimulated by contributions from numerous individuals throughout the solar physics and astrophysics communities. Extensive discussion and review have come from **NASA** working groups and study teams, in particular: the Hard X-ray Imaging Instrument (**HXII**) Facility Definition Team led by L. E. Peterson; the Pinhole/Occulter Facility (**P/OF**) Science Working Group led originally by E. Tandberg-Hanssen and H. R. Hudson and more recently by J. M. Davis and H. R. Hudson; and the MAX '91 Science Study Committee led by B. R. Dennis. Further concept development was contributed by the members of the team, headed by T. A. Prince, that proposed **GRID** for the Solar High-energy Astrophysical Plasmas Explorer (SHAPE) mission. **HEIDI** is an adaptation of the **GRID** on a Balloon payload that was originally selected for **NASA**'s Max '91 Program and then cancelled. The **HEIDI** team is working closely with the **HESP** Science Study Group

chaired by R. P. Lin, with B. R. Dennis as study scientist.

This work was supported in part by **NASA** RTOP 370-04-07 and NSG 5066. At Caltech this work is supported by **NASA** under NAS5-30792. Undergraduate students working on the **HEIDI** project were supported in part by NSF Grant Number ATM 9100614.

The flight electronics subsystem for **HEIDI** is being developed at Goddard with the assistance of T. Plummer, B. Muney, J. Novello, C. Condor, and C. Nash. The design and fabrication of the gondola, telescope structure, and grids is being carried out at Goddard with the assistance of R. Dame, K. Segal, D. Clark, W. Nagel, L. White, C. Shields, and D. Linard. Characterization of the grids at Goddard is being done with the assistance of J. Hagopian and J. Crook. The GSE software is being written by P. Kenny at Goddard. Students who have worked on **HEIDI** at Goddard include E. Korenic, V. Glasgow, E. Tan, M. Amato, L. Olah, T. Hodge, P. Uribe, and C. Purvance. The assistance of S. Gross at Auburn University with the interface between the pointing control subsystem and the mechanical structures and the role of R. Goeden at Caltech in the design and fabrication of the **OPAS** system are gratefully acknowleged.

VI. Bibliographical References

[1]Tandberg-Hanssen, E. A., H. S. Hudson, J. R. Dabbs, and W. A. Baity, "The Pinhole/Occulter Facility", **NASA** TP, 1983.

[2]Crannell, C. J., G. J. Hurford, L. E. Orwig, and T. A. Prince, "A Fourier Transform Telescope for Sub-Arc Second Imaging of X Rays and Gamma Rays", *SPIE* **571** (1985) 142.

[3]Prince, T. A., G. J. Hurford, H. R. Hudson, and C. J. Crannell, "Gamma-Ray and Hard X-Ray Imaging of Solar Flares", *Solar Phys.* **118** (1988) 269-290.

[4]Thompson, A. R., J. M. Moran, and G. W. Swensen Jr., "Interferometry and Synthesis in Radio Astronomy," Krieger Publishing Company, Malabar, Florida, 1991.

[5]Lindsey, Charles A. "Effects of Diffraction in Multiple-Grid Telescopes for X-Ray Astronomy," *J. O. S. A.* **68** (1978) 1708–1715.